Rotationally Resolved Electronic Spectra of 1-Methoxynaphthalene

in the Gas Phase

by

Seung-hoon Hong

B.S., Korea University, 1997

M.S., Korea University, 2000

Submitted to the Graduate Faculty of

Arts and Science in partial fulfillment

of the requirements for the degree of

Master in Science

University of Pittsburgh

2005

UNIVERSITY OF PITTSBURGH

THE SCHOOL OF ARTS AND SCIENCES

This thesis was presented

by

Seung-hoon Hong

It was defended on

February 4th, 2005

and approved by

David H. Waldeck, Professor, Department of Chemistry

Sunil Saxena, Assistant Professor, Department of Chemistry

David W. Pratt, Professor, Department of Chemistry, Thesis Director

Rotationally Resolved Electronic Spectra of
1-Methoxynaphthalene in the Gas Phase

Seung-hoon Hong, M.S.

Abstract.

Rotationally resolved fluorescence excitation spectra of the 0_0^0 band of the $S_1 \leftarrow S_0$ transition of 1-methoxynaphthalene have been observed using a high resolution laser spectrometer operating in the ultraviolet. The *trans*-1-methoxynaphthalene band is an *ab* hybrid band with 38% *a*-type character and 62% *b*-type character. The band origin is at 31671.7 cm^{-1}, and the rotational constants are A" = 1643.98, B" = 832.62 and, C" = 554.83 MHz in the ground state, and A' = 1626.6, B' = 818.5, and C'= 546.6 MHz in the excited state. Two other bands at +16 and −70 cm^{-1} from the origin band of *trans*-1-methoxynaphthalene exhibit a band head shape. The possibility of a perpendicular conformer as being the source of these bands is discussed.

TABLE OF CONTENTS

LIST OF TABLES

LIST OF FIGURES

To my father who passed away a month ago

1. **Instrument**

1.1. **Introduction**

The rotationally resolved electronic spectra presented in this thesis were obtained using a high resolution CW laser/molecular beam spectrometer. A schematic diagram of the spectrometer is shown in Figure 1; it is described in detail elsewhere [1, 2].

Briefly, a molecular beam is generated by passing Ar or He as a carrier gas through a heated quartz source containing the sample in a first vacuum chamber of at about 10^{-4} torr. Then, the gas is expanded through a nozzle into a differentially pumped second vacuum chamber ($\sim 10^{-6}$ torr). The beam is skimmed by a 1 mm skimmer located 2 cm downstream from the nozzle before it is expanded into a third higher vacuum chamber. The frequency doubled UV light from a single frequency CW Ar^+ pumped ring dye laser crosses the molecular beam 15 cm or 110 cm downstream from a nozzle at right angles from a molecular beam. The LIF spectrum of the sample is collected and detected at right angles to both the molecular and laser beam as a function of the laser frequency by a photomultiplier tube (PMT) and data acquisition system. Along with the LIF spectrum, an iodine absorption spectrum and relative frequency markers is simultaneously collected for frequency calibrations.

The primary components of the high resolution CW laser/molecular beam spectrometer are the CW ring dye laser, the molecular beam machine, and the light detection ststem which are described in detail in the following section.
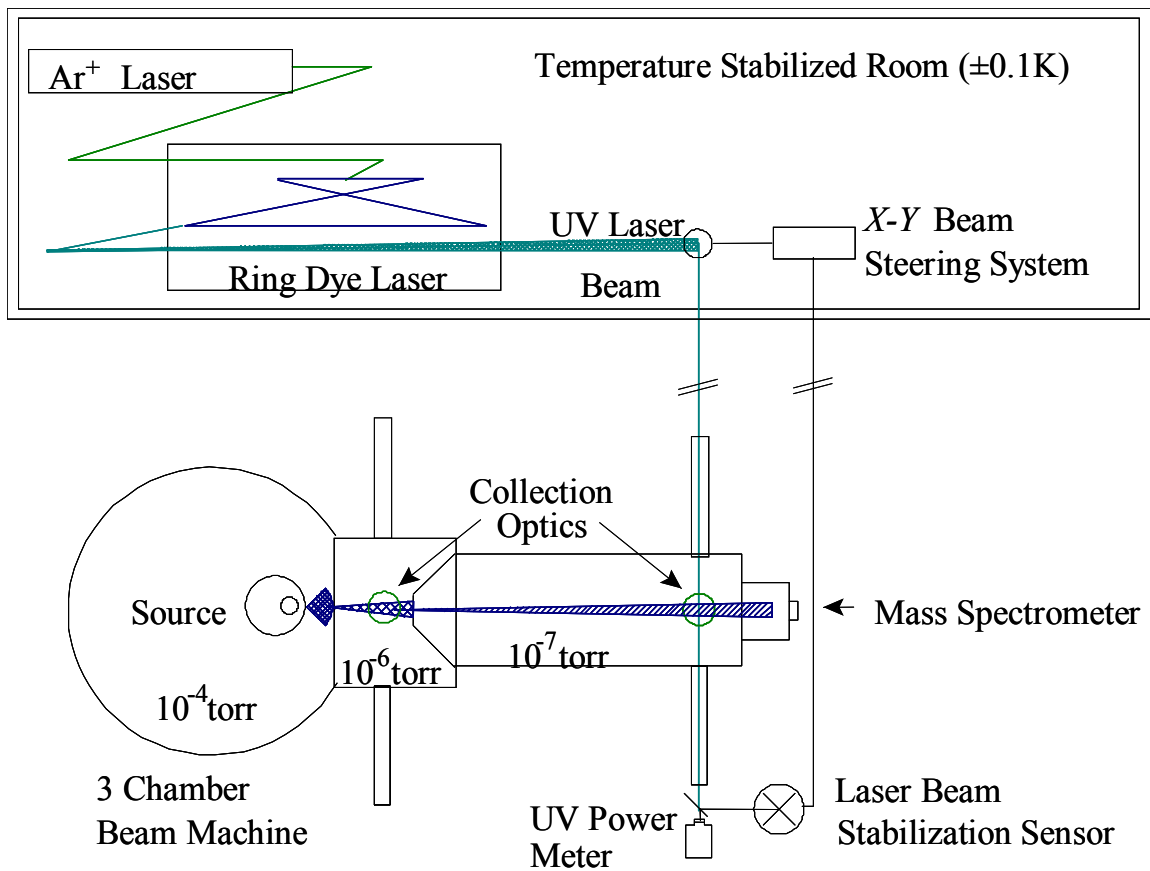
Figure 1. Overall layout of the high resolution laser spectrometer.

The figure contains the following labels:

- Ar$^+$ Laser
- Temperature Stabilized Room (±0.1K)
- Ring Dye Laser
- UV Laser Beam
- X-Y Beam Steering System
- Collection Optics
- Source
- Mass Spectrometer
- 10^{-4}torr
- 10^{-6}torr
- 10^{-7}torr
- 3 Chamber Beam Machine
- UV Power Meter
- Laser Beam Stabilization Sensor

1.2. CW ring dye laser

The CW ring dye laser system (Spectra Physics Model 380D) is shown in Figures 2 and 3. The CW ring dye laser and its peripheral devices rest on a vibrationally isolated table (Newport 12 x 5 x 1.5 ft). Three legs of the table are equipped with 11 vibration isolators (Berry Model SLM-3) which damp building vibrations.

The CW ring dye laser has been modified from its original structure. Micrometers accessible from outside the laser cavity replace the original mirror adjusters. A doubling crystal assembly has been installed at the auxiliary beam waist for UV light generation. To increase the frequency specificity, various optical elements and electronics were added into the cavity. The metal cover has been replaced with a Plexiglas cover to allow visual alignment of the laser while maintaining nitrogen atmosphere within the laser cavity.

The components in the ring dye laser cavity are shown in Figure 2. The Ar^+ pump beam is generated by a Spectra Physics Model 171 Ar^+ laser which operates in its single frequency mode at 514.5 nm. Typical power output from the Ar^+ pump laser is about 5 W. This 514.5 nm line of the Ar^+ pump laser is guided by a pump mirror and focused on a dye jet containing dyes in viscous solvents. The laser cavity consists of four mirrors and has two foci. The dye jet is positioned at one focus and a Brewster-angle cut or perpendicular-incidence cut doubling crystal ($LiIO_3$ or BBO) is positioned at the other focus.
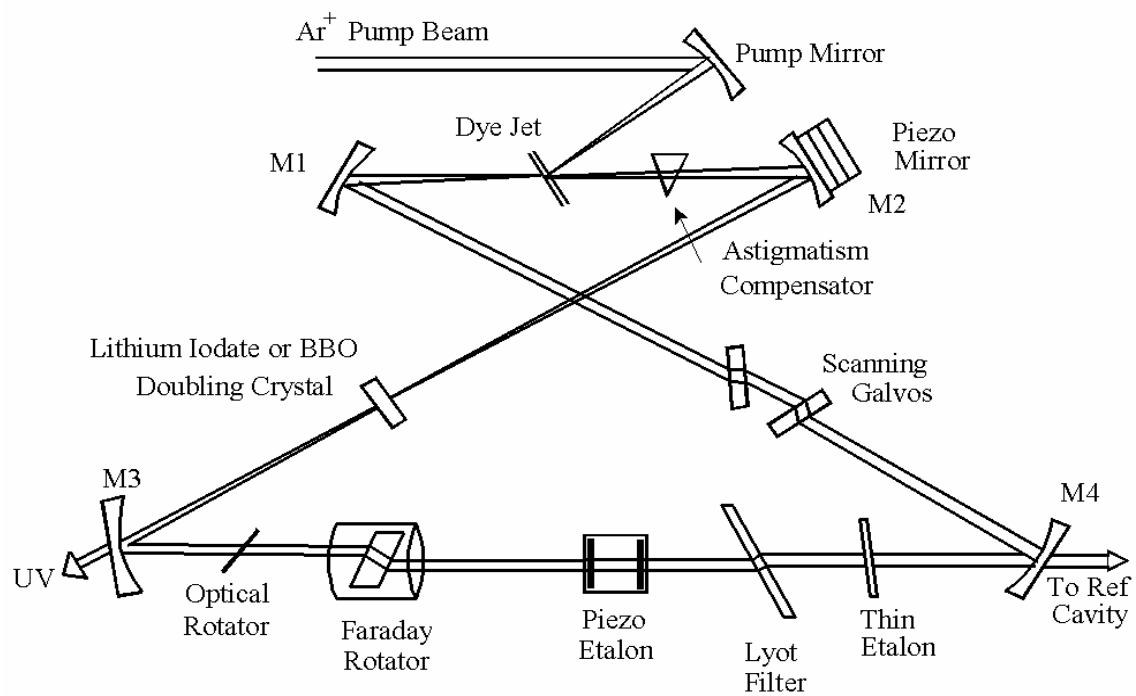
Figure 2. Schematic diagram of the high resolution CW ring dye laser.
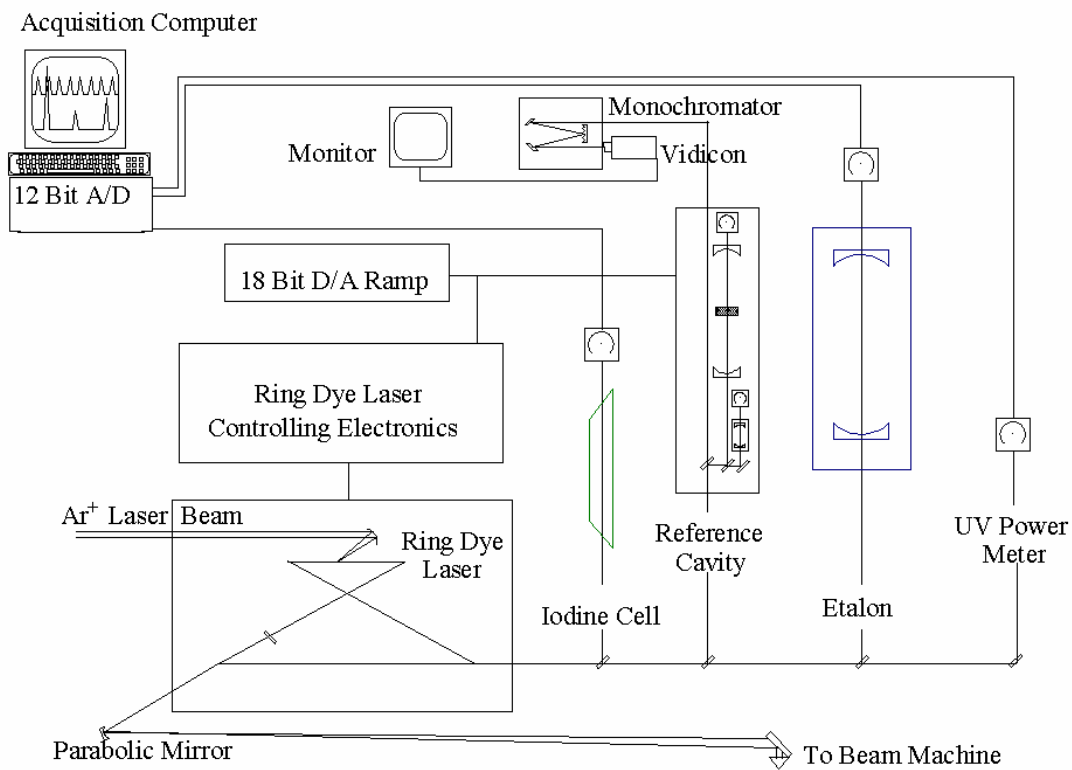
Figure 3. Schematic diagram of the stabilization system.

A pair of galvo plates is used to scan the frequency. The galvo plate inside the reference interferometer was replaced with a bigger and more rotatable one to extend the scan range. Two of the three plates of the birefringent filter (Lyot filter) were removed to flatten its transmission curve. Then, the 900 GHz thin plate etalon was made to follow the scan by mounting it on a galvanometer that can be tuned by the same voltage ramp that tunes the 75 GHz piezo scanned thick etalon. These optical elements act as optical frequency bandpass filters that narrow the range of the lasing frequencies until only one 200 MHz cavity mode remains above threshold. Frequency stabilization is accomplished with a 0.5 GHz reference interferometer (reference cavity) in which a galvo plate is scanned simultaneously with the galvo plates in the ring dye laser cavity. When mode hop occurs, the reference cavity voltage jumps and the lock is broken, at which time the 10 GHz interferometer slave cavity and the reference cavity lengths are temporarily frozen. Mode locking is achieved by a slave cavity which sends an error signal to the M2 mirror to bring the laser back to the selected mode. Then, lock is again established and the laser frequency returns to where it was before the lock was broken.

Frequency calibration of a spectrum is accomplished using the iodine absorption spectrum for absolute frequency calibration and an interferometer for relative frequency calibration. The absolute frequencies of the iodine transitions were provided by the iodine atlas [3]. An iodine cell is simultaneously scanned by a diverted portion of the fundamental laser beam and recorded by the data acquisition computer. The uncertainty of the absolute frequency calibration in the UV is about 0.001 cm^{-1}. The Fabry-Perot interferometer is also scanned simultaneously in the fundamental laser beam and generates fringe signals to provide the relative frequency standard. The free spectral range between two consecutive fringes is 599.5040 MHz. Since the marker

frequency stability and free spectral range are sensitive to the temperature, the temperature of the laser room is controlled by Honeywell Model UCD 5000 PID digital controller to within ±0.1 $^{\circ}$C.

1.3. Molecular beam machine and light detection system

A diagram of a molecular beam machine is shown in Figure 4. This machine provides a highly collimated supersonic molecular beam, making possible detection of laser induced fluorescence from a spatially selective region where the laser and the molecular beam cross. As shown in Figure 4, the machine consists of three differentially pumped vacuum chambers; the source chamber, the buffer chamber, and the research chamber in order of increasing vacuum. These three chambers are separated by 1 mm skimmers which are used to collimate the molecular beam and to limit the molecular flow into the buffer and research chamber. The molecular beam formed in the source chamber travels through the skimmers to the buffer chamber and research chamber where the molecular beam is crossed and excited by the laser beam. In this arrangement, the pressure in each chamber is maintained such that the mean free path of the carrier gas is larger than the distance the molecular beam travels in that chamber. This creates a collision-free environment in the molecular beam after the expansion.

A diagram of the molecular source with the collection optics is shown in Figure 5. The source is made of quartz and consists of three sections, each of which is wrapped with thermocouple wire (NiCr/CuNi) to measure the temperature and 0.5 mm platinum coaxial heating wires to increase the temperature to as high as 400 $^{\circ}$C. The temperature is controlled independently for each section. The top section is used to hold the sample, and the middle
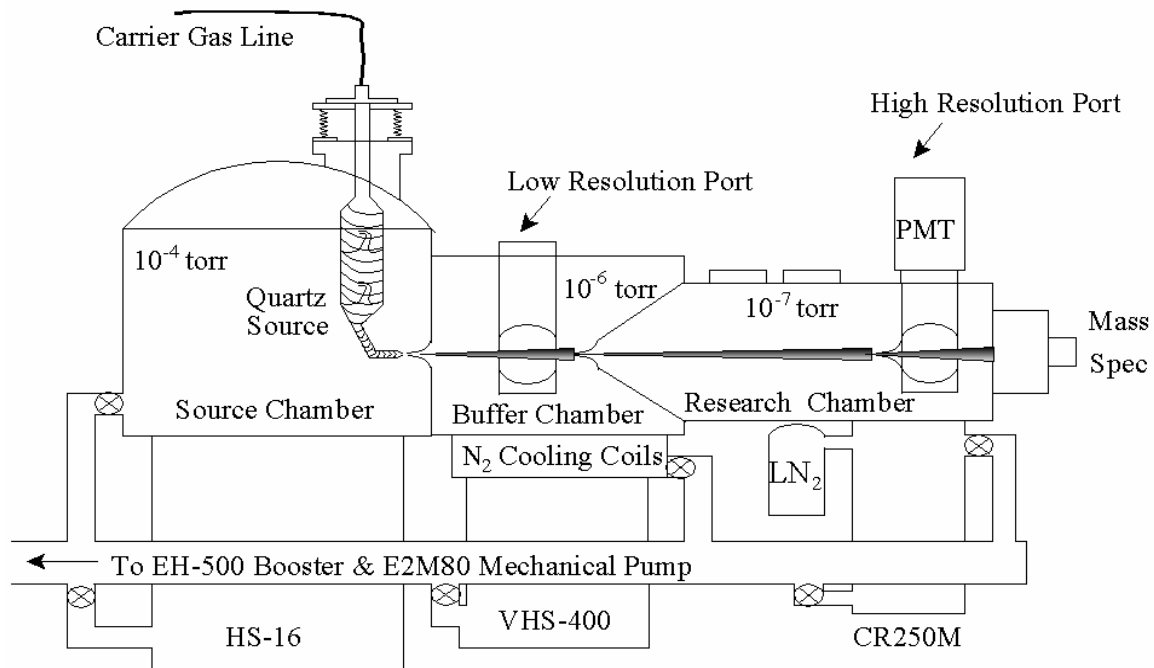
Figure 4. Schematic diagram of the molecular beam machine.
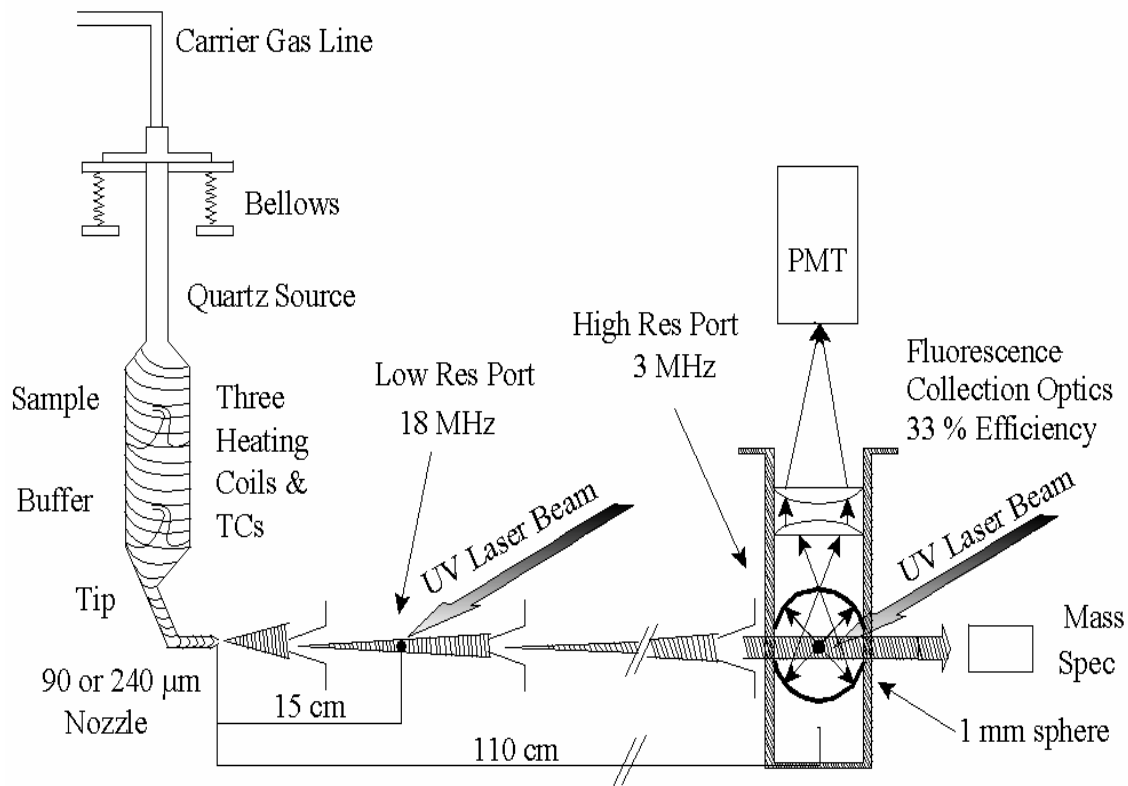
Figure 5. Schematic diagram of the molecular source and the collection optics.

section provides a trap for particles to prevent the nozzle from clogging. The nozzle diameter of the source is 240 μm.

The buffer and research chamber each provide a region to cross the molecular beam with the laser beam. The crossing region is either 15 cm downstream from the nozzle in the buffer chamber or 110 cm downstream from the nozzle in the research chamber. A set of collection optics can be positioned at each of the crossing regions. When the fluorescence signal is strong, the collection optics are positioned at the research chamber site to minimize Doppler broadening. When the fluorescence signal is weak, the spectrum is taken at the buffer chamber to increase the S/N ratio. The collection optics provide spatial filtering of the laser induced fluorescence signal. The effective collection volume is about 1 mm^3.

The Doppler linewidth of this apparatus can be estimated using the equation [4]

$$\delta\nu_{FWHM} = 2\sqrt{\ln 2}\,\nu_0\,\frac{d}{z}\frac{v}{c}$$

where ν_0 is the excitation frequency, d is the collection volume diameter, z is the distance downstream of the source, v is the molecular beam velocity, and c is light velocity. For a Ar as a carrier gas, the measured velocity is 500 m/sec and when the excitation frequency of the laser is 33,000 cm^{-1}, the Doppler linewidth in the research chamber is calculated to be

$$\delta\nu_{FWHM} = 2\sqrt{\ln 2}\,x\,9x10^{14}\,xMHzx\,\frac{1mm}{1100mm}\frac{500m/\sec}{3x10^8\,m/\sec} = 2.0\,MHz$$

In addition to the narrow band width of the laser and the collision-free environment, the resolving power of the spectrometer is determined by its light detection system. It employs a two-mirror setup to collect fluorescence and a condenser-PMT combination to detect photons. The two spherical mirrors have equal radii. The collection volume is located at the spherical center of the top mirror. The bottom mirror is placed in such a way that it focuses the collection volume to a small aperture located at the center of the top mirror. The collection efficiency is about 33%. The photons collected by the mirror setup are focused onto the PMT by the condenser. The PMT signals generated by photons are sent to EG&G PAR 1121A amplifier/discriminator and then processed by a PAR 1112 photon counter. The number of counts accumulated is then acquired by JB 95 program for recording.

With this high resolution apparatus, total molecular fluorescence, total UV power, the iodine absorption spectrum, and the markers from the 600 MHz interferometer are acquired. These data are digitized and recorded with the JB 95 program as a function of the dye laser frequency.

1.4.   References

[1] Majewski, W. A.; Pfanstiel, J. F.; Plusquellic, D. F.; Pratt, D. W. *Laser Techniques In Chemistry*, John Wiley & Sons, Inc. **1995**, 101

[2] Majewski, W. A.; Plusquellic, D. F.; Pratt, D. W. *J. Chem. Phys.* **1989**, *90*, 1362

[3] Gerstenkorn, S. ; Luc, P. *Atlas du spectroscopie d'absorption de la molecule d'iode*, CNRS, Paris, **1978** and **1982**

[4] Demtroder, W. *Laser Spectroscopy*, Springer-Verlag, Berlin Heidelberg, **1982**

2. High resolution electronic spectra of 1-methoxynaphthalene in the gas phase

2.1. Introduction

Narrow band UV lasers in combination with supersonic molecular beams are very powerful tools in molecular spectroscopy. Much information about a molecule such as its structure and dynamical properties in both ground and electronically excited states can be obtained by this technique [1]. When organic molecules are seeded in a carrier gas such as He and Ar, and expanded into a high vacuum chamber, most of the vibrational degrees of freedom are quenched. Then, only the rotational levels in the electronic ground state are populated leading to less congested fluorescence spectra when the molecule is excited by the UV laser.

Molecular constants obtained from the analysis of rotationally resolved laser induced fluorescence (LIF) spectra are directly related to the molecular structure in both ground and excited states. Different conformers can be identified when rotational constants are available for each conformer.

Much research concerning aromatic methyl ethers has been performed to understand their conformational behavior. The torsional motion of methoxy group of the anisole with respect to the plane of the aromatic ring (see below) was a main interest [2-5]. Although a molecule like
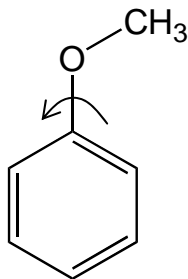
anisole prefers the planar conformation energetically, rather than a nonplanar conformation, the possible existence of stable second conformer has been controversial. A two-fold barrier opposing the internal rotation of anisole has been reported in many experimental studies, where planar conformer is energetically more favored than the nonplanar conformer by 3.6 ~ 5.7 kcal/mol [2, 3]. Microwave studies observed only the planar conformation of anisole in the ground state, and found no lines for second conformer, possibly because many lines of vibrationally excited states obscure its transitions [6]. Also, a recent jet-cooled high resolution study reported only the planar conformation of anisole both in the ground state and first excited state, from the band contour and line fittings [7].

However, NMR studies of anisole reported that the barrier for methoxy internal rotation is both two-fold and four-fold in nature, which indicates the existence of second stable conformer [8]. Theoretical calculations have reported a relatively low energy barrier to rotation of the methoxy group and agreed on the second conformer [9, 10]. The energy barrier between two stable conformers was reported to lie in the range of 1 ~ 2.1 kcal/mol depending on the calculation method.

Troxler, *et al.* [11] have reported a study of jet-cooled 2-methoxynaphthalene. Two rotational isomers were found; two coplanar from of *trans* and *cis* conformations. Unlike 2-hydroxynaphthalene, where *cis* and *trans* conformers were reported in the 2:1 ratio [12], 2-methoxynaphthalene mostly exists as a *cis* conformation. Two rotational isomers were also reported for 1-hydroxynaphthalene and they are ascribed to both planar *cis* and *trans* conformations [13]. In this case most of the 1-hydroxynaphthalene molecules exist as the *trans* conformer.

Recently, Mahato, *et al.* [14] reported a UV laser spectroscopy study of 1-methoxynaphthalene in a supersonic jet expansion, combined with *ab initio* theoretical calculations. Two rotational isomers of 1-methoxynaphthalene have been identified and assigned as a planar *trans* conformer, and a perpendicular conformer with the methoxy group out of the aromatic ring plane. *Ab initio* theoretical calculations supported the existence of a perpendicular conformer over the *cis* conformer, as the energy barrier between the *trans* conformer and the perpendicular conformer was reported as 2.1 kcal/mol while it is 11 kcal/mol between *trans* and *cis* conformers. This conformational difference can be studied and understood by high resolution UV spectroscopy, where the existence of perpendicular conformer with respect to the aromatic ring may be detected.

2.2. Experimental

High resolution data were obtained using the CW ring dye laser with the molecular beam machine described in the previous section. 1-Methoxynaphthalene was purchased from Aldrich (98% + pure) and used without further purification. A DCM dye in benzyl alcohol, DMSO, and glycerol (2:3:3 ratio) was used for the ring dye laser. The Brewster-angle cut lithium iodate ($LiIO_3$) crystal was used for intracavity frequency doubling. 1-Methoxynaphthalene was seeded in Ar or He carrier gas and expanded through a 240 μm quartz nozzle, skimmed once, and probed 15 cm downstream of the nozzle in the buffer chamber by the frequency doubled ring dye laser beam. Fluorescence was collected using spatially selective optics, detected by a photomultiplier tube and photon counting system, and processed by a computerized data acquisition system. Relative frequency calibrations of the spectra were achieved by using a

interferometer having a mode-matched FSR of 299.7520 ± 0.0005 MHz at the fundamental frequency of the dye laser. Absolute frequency calibration was performed using the electronic absorption spectrum of iodine.

2.3.   Results

A low resolution $S_1 \leftarrow S_0$ laser induced fluorescence (LIF) excitation spectrum of jet-cooled 1-methoxynaphthalene taken by Das, *et al.* [15] is shown in Figure 6(a). They assigned the strongest band in the spectrum at 31685 cm^{-1} to the electronic origin (0_0^0) of the *trans* conformer, and the much weaker band at 31610 cm^{-1} to the electronic origin of the less stable *cis* conformer, as the case of 1-hydroxynaphthalene. But in a later LIF study [14], they reported a different assignment for the weaker band.

A number of weak features around the strong origin band are magnified and illustrated in Figure 6(b). Weak features to the red of the origin band were attributed to a progression and combination of two low frequency vibrations of 22 and 28 cm^{-1}, as shown in the figure. These weak features to the red of the electronic origin of the *trans* conformer were very dependent on the backing pressure of the carrier gas. They appeared only when the backing pressure of the carrier gas was high, so the cooling was effective. When backing pressure was low, these patterns disappeared and a new set of transitions appeared which was ascribed to hot band and sequence bands. Also, Das, *et al.* [15] found that the feature at $0_0^0 + 15$ cm^{-1} is present under all expansion conditions. Combined with dispersed fluorescence, and *ab initio* calculation, they

(a)

0_0^0 (trans)

0_0^0 (cis)

Intensity

Wavenumber (cm⁻¹)
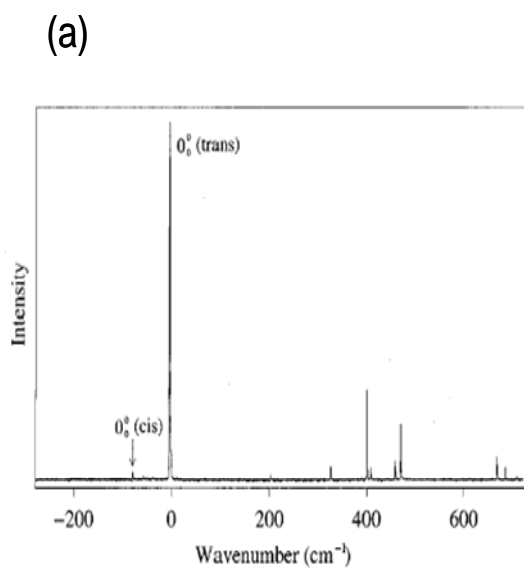
J. Chem. Phys. **2001**, *114*, 8310, Das et al.

(b)

22.3 20.5 18.5

A_0^0 A_0^1 A_0^2 A_0^3

B_0^1 $B_0^1 A_0^1$ $B_0^1 A_0^2$

C_0^1

a
b
c
d

Intensity

Wavenumber (cm⁻¹)
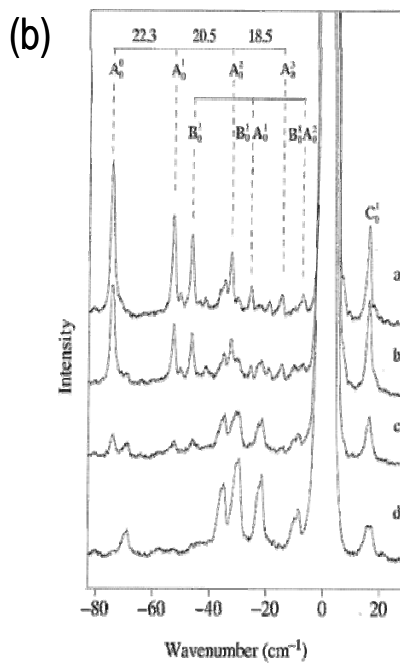
J.Phys.Chem.A, **2002**, *106*, 12058, Mahoto et al.

Figure 6. (a) Low resolution fluorescence excitation spectrum of 1-methoxynaphthalene in the origin band region at 31685 cm⁻¹ (b) Fluorescence excitation spectra of 1-methoxynaphthalene at different backing pressures of He: a) 30, b) 20, c) 10, and d) 5 psi.

assigned the $0^0_0 - 75$ cm^{-1} band to the electronic origin of an out-of plane 1-methoxynaphthalene, in which the methoxy group is perpendicular to the naphthalene ring, and the $0^0_0 + 15$ cm^{-1} band to one quantum of excitation of the torsional motion of the methoxy group with respect to the naphthalene ring. Our high resolution study of these three different bands, the strong band, the $0^0_0 - 75$ cm^{-1} band, and the $0^0_0 + 15$ cm^{-1} band will be discussed in the following sections.

2.3.1.   High resolution electronic spectrum of *trans*-1-methoxynaphthalene

A rotationally resolved $S_1 \leftarrow S_0$ fluorescence spectrum of the strong band was obtained at 31672 cm^{-1} using Ar as a carrier gas at -14 psi while heating the sample to about 388 K. This spectrum is shown in Figure 7(a). This band spans approximately 2 cm^{-1}. The spectrum shows two well-defined branches at lower and higher energy regions of the spectrum, and it also shows a relatively small branch in the middle energy range of the spectrum. The lower frequency branch is a P-branch ($\Delta J = -1$), the higher frequency branch is an R-branch ($\Delta J = +1$), and the branch in the middle is a Q-branch ($\Delta J = 0$). A relatively smaller Q-branch in the middle of the spectrum indicates that the spectrum is an *ab* hybrid type spectrum.

This spectrum could be analyzed and understood by using the rigid rotor Hamiltonian,

$$H_r = AP_a^2 + BP_b^2 + CP_c^2$$

where P_a, P_b, P_c are the components of the angular momentum about the principal axes of inertia, *a, b, c* respectively. These inertial axes are fixed with the molecule with origin at the center of the mass of the molecule. Their orientation is determined by the coordinates of the nuclei only;

(a) Experimental

31670.59 cm^{-1}

31672.58 cm-1
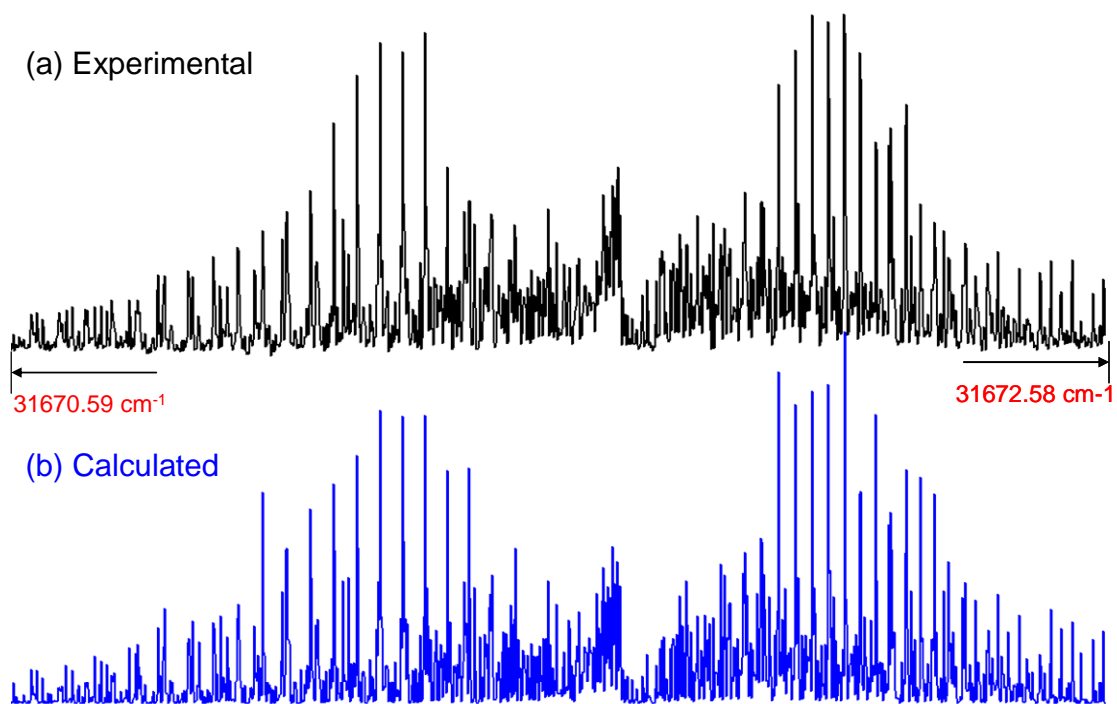
(b) Calculated

Figure 7. Rotationally resolved fluorescence excitation spectra of the origin band of *trans*-1-methoxynaphthalene (a) Experimental (b) Calculated.

the coordinates of the electrons are not involved. A, B, and C are rotational constants corresponding to the inertial axes, and they are defined below:

$$A = \frac{h}{8\pi^2 I_a}; \quad B = \frac{h}{8\pi^2 I_b}; \quad C = \frac{h}{8\pi^2 I_c}$$

Here, I_a, I_b, and I_c are the principal moments of inertia.

The spectral fitting was done with the JB95 program with two sets of rotational constants, three rotational constants for the ground state and excited state, respectively, as starting parameters for the fit. *Ab initio* geometry optimizations of the ground state of different conformers of 1-methoxynaphthalene were done at the MP2/6-31G** level. From this calculation, we obtained theoretical rotational constants of the electronic ground state for each conformer. Also, geometry-optimized CIS/6-31G** calculations were performed to obtain theoretical rotational constants of the electronic excited state. These two sets of theoretical rotational constants were used as starting values for the fit. Later, these theoretical rotational constants will be compared to the experimental rotational constants obtained from the fit.

The JB95 program, based on the prolate type rigid rotor, generates a simulated line set consisting of a band type label, six quantum numbers (J'', K_a'', K_c'', J', K_a', K_c'), and a simulated frequency and intensity for each line. There are two fitting strategies to refine the model parameters. The first method is to match the spectral pattern by regenerating a simulated spectrum through step-wise parameter adjustment. The second method is using linear least squares regression following quantum number assignments of the experimental frequencies. This process begins with the creation of an assignment file that contains a list of experimental

frequencies and the associated quantum number labels. Selection of a specific line from the spectrum is used for assiging and deleting the associated experimental frequency. A collection of assigned lines is then used to minimize the observed minus calculated (OMC) standard deviation using a least square procedure. The intensity of the lines is fit by changing rotational temperature of the molecule and also by changing the transition dipole moment ratio (*a*, *b*, or *c* type) which is particularly useful if the orientation of the transition moment is not known. Also, each simulated line is convoluted with a Gaussian, Lorentzian, or Voigt lineshape function to match the experimental data. Rovibronic transitions of as many as 155 lines were assigned for the spectrum with a OMC of 3.4 MHz for the frequency fit. The calculated electronic spectrum is shown in Figure 7(b).

A fully resolved spectrum of a portion of the P-branch is shown in Figure 8. The top trace is the experimental spectrum and the bottom trace is the calculated spectrum. The linewidth (FWHM) of single transition peaks is measured to be 26 MHz. The similarity between two spectra shows the quality of the fit. The Gaussian linewidth caused by Doppler broadening of the peak was determined to be 18 MHz and the Lorentzian linewidthscaused by the lifetime broadening was determined to be 13 MHz. Together, a Voigt profile explains the 26 MHz linewidth of individual lines in the spectra peak. The rotational temperature of the molecule was determined to be 4 K.

Along with parameters described above, we obtained the rotational constants of the molecule in its ground and excited states. These constants are listed in Table 1, together with the theoretical rotational constants obtained from the *ab initio* calculations for *trans*-1-methoxynaphthalene. The *ab initio* values of the ground state rotational constants of *trans*-1-methoxynaphthalene are very similar to the experimental rotational constants.

FWHM = 26 MHz

0.08 cm^{-1}
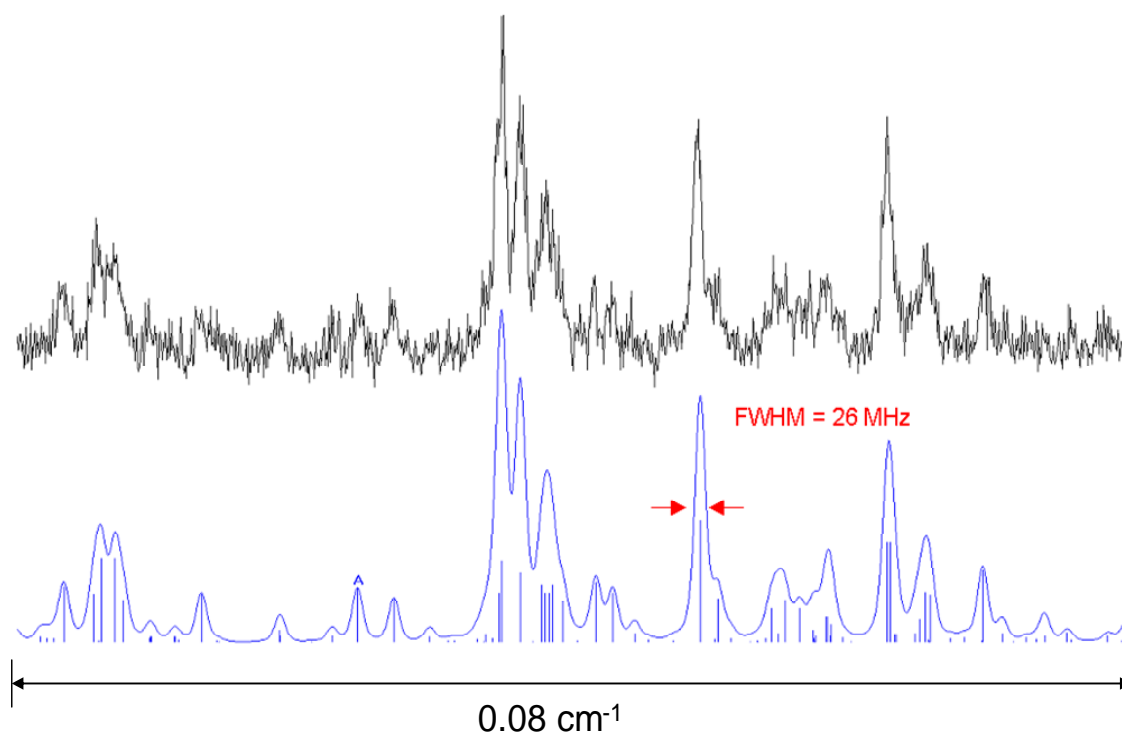
Figure 8. A portion of the rotationally resolved fluorescence excitation spectrum of the origin band of *trans*-1-methoxynaphthalene, extracted from the P-branch.

Table 1. Theoretical and experimental parameters of *trans*-1-methoxynaphthalene**.** The *ab initio* geometry optimization in the ground state was done at the MP2/6-31G** level. A geometry optimized CIS/6-31G** calculation was performed to obtain the theoretical rotational constants of the electronic excited state.

	Theoretical parameters	Experimental parameters
Ground State		
A" (MHz)	1641.79	1644.0(1)
B" (MHz)	831.88	832.6(1)
C" (MHz)	554.08	554.8(1)
ΔI (amuÅ2)	-3.197	-3.519
κ	-0.49	-0.49
Excited State		
A' (MHz)	1656.73	1626.6(1)
B' (MHz)	827.71	818.5(1)
C' (MHz)	553.86	546.6 (1)
ΔI (amuÅ2)	-3.164	-3.605
κ	-0.503	–0.496

The inertial defect is a difference in the principal moments of inertia, and is defined below:

$$\Delta I = I_c - I_a - I_b$$

It is a measurement of the planarity of the molecule. For a planar molecule it is close to zero and for nonplanar molecules it becomes more negative. From the experimental result the inertial defect is measured as -3.519 amuÅ^2. This value is more negative than that of *trans*-1-hydroxynaphthalene ($\Delta I = -0.204$ amuÅ^2) [12] due to the two methoxy group hydrogens out of the plane. This inertial defect can be compared with the planar conformation of anisole where inertial defect is -3.410 amuÅ^2 [6]. From the inertial defect we can conclude that this conformer of *trans*-1-methoxynaphthalene has a planar geometry in ground state.

The asymmetry parameter κ is given by the equation below

$$\kappa = (2B - A - C) / (A - C))$$

For a prolate symmetric rotor B = C and $\kappa = -1$, and for an oblate symmetric rotor A = B, and κ = 1. For a totally asymmetric rotor κ = 0. From the experimental rotational constants it is measured as -0.490 indicating the molecular geometry is near prolate.

The rotational constants for the electronically excited state are measured as A' = 1643.98, B' = 832.62, and C'= 554.83 MHz, respectively. Although the calculated rotational constants show a larger deviation from the experimental constants than do those of the ground state, they are still in good agreement, within the error range of 1.9 %. The rotational constant changes are $\Delta A = -17.41$, $\Delta B = -14.11$, and $\Delta C = -8.2$ MHz. The decreased values indicate that the displacements

of atoms with respect to each of the *a, b, c* inertial axes are increased upon excitation because rotational constants are inversely proportional to the moments of inertia. Since the changes are small, the geometry of the electronically excited state is similar to the geometry of the ground state. The small change of inertial defect ($\Delta\Delta I = -0.086$ amuÅ^2) supports the similarity of the molecular structure between the ground and excited state. From this rotational analysis of the strongest band at 31672 cm-1, this band is now assigned as *trans*-1-methoxynaphthalene.


2.3.2.   High resolution electronic spectra of the +16 cm^{-1} and –70 cm^{-1} bands

Another rotationally resolved fluorescence excitation spectrum was obtained at 31688 (+16) cm^{-1} using He as a carrier gas while heating the sample to about 400 K. This spectrum was obtained when the backing pressure was -20 psi and is shown in Figure 9.

This band has very strange shape. The intensity of the spectrum suddenly increases in the high wavenumber region. Then, right after a strong peak, the intensity dropp quickly towards zero and there are no significant transitions obtained beyond this point. At lower frequencies, there is first a long series of peaks with separations varying from 320 to 920 MHz, then a low intensity region, and finally a series of low intensity peaks separated by larger frequencies. The band shape is very different from the origin band of the *trans* conformer in Figure 6(a), which suggests that this band may be ascribed to a different conformer. As stated earlier, Mahato *et al*. [14] assigned this band to one quantum of excitation in the torsional motion of the methoxy group with respect to the naphthalene ring.

A second weak spectrum was obtained at 31602 (–70) cm^{-1} using He as a carrier gas while heating the sample to about 387 K. Unlike the previous result by Mahato *et al*. [14], no noticeable signal was found at higher backing pressure in our experiment. Instead, when the

3.23 cm^{-1}
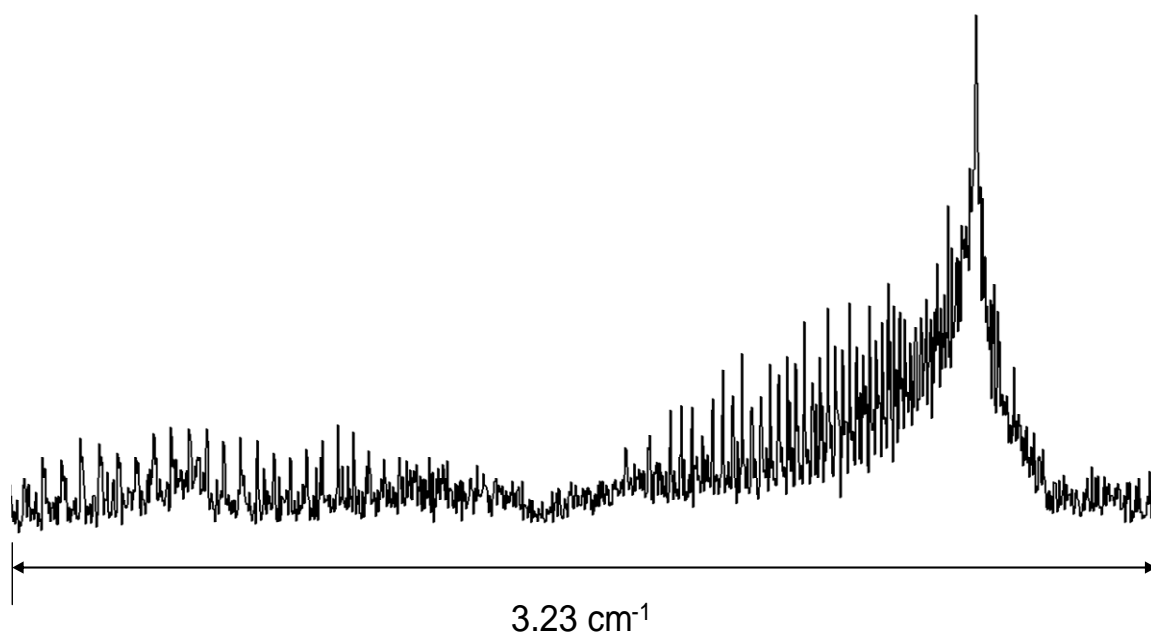
Figure 9. Rotationally resolved fluorescence excitation spectrum of the +16 cm^{-1} band of *trans*-1-methoxynaphthalene.
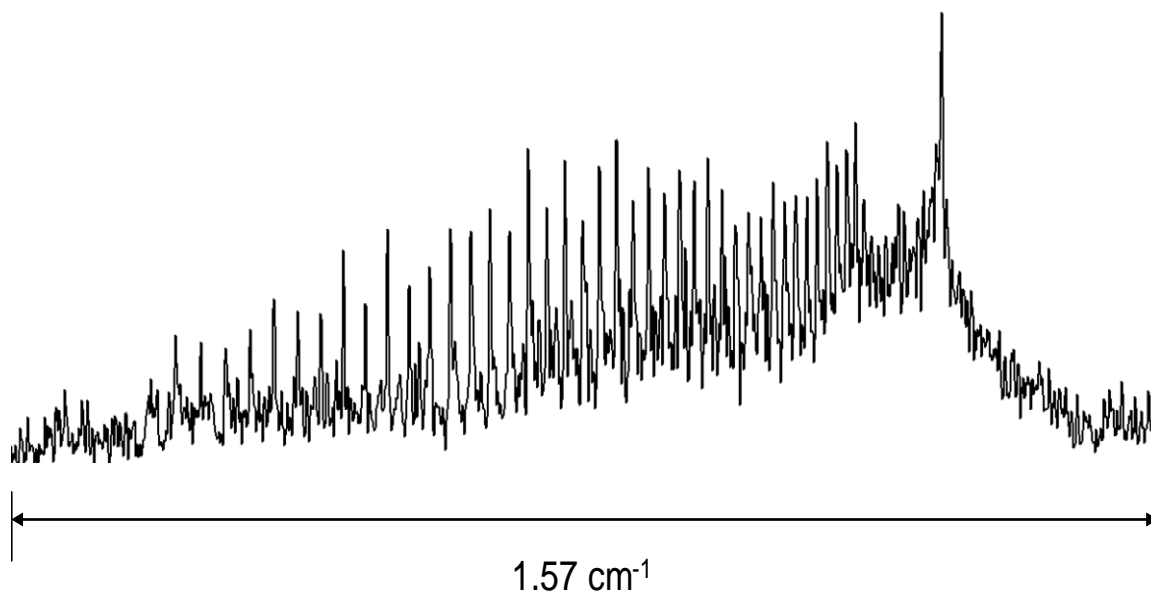
**Figure 10. Rotationally resolved fluorescence excitation spectrum of the –70 cm^{-1} band of *trans*-1-methoxynaphthalene.**

backing pressure was lowered to –18 psi with He as a carrier gas, a spectrum at –70 cm^{-1} from the *trans* origin was obtained. This spectrum is shown in Figure 10. Since no other noticeable features were found to the red of the origin band of the *trans* conformer, the –70 cm^{-1} band is believed to be the –75 cm^{-1} band in the low resolution study which is the strongest band among those weak features seen in Figure 6(b). Therefore, we assume that –70 cm^{-1} band may be ascribed to a perpendicular conformer of 1-methoxynaphthalene based on the previous low resolution study. Rotational analysis of the spectrum will be necessary to prove than this assignment is correct.

One interesting feature of this band is its similarity to the +16 cm^{-1} band. The –70 cm^{-1} band also has sharp strong peak in the high wavenumber region, and a long series of peaks with separations varying from 340 to 950 MHz at lower frequency. The –70 cm^{-1} band spans approximately 1.6 cm^{-1} while the +16 cm^{-1} band spans approximately 3.2 cm^{-1}. Since the –70 cm^{-1} band shows no P-branch whereas the +16 cm^{-1} band does, we may say that only part of the –70 cm^{-1} band was recorded, possibly due to the very weak intensity of the P-branch region of the spectrum. Due to the difficulties caused by weak intensity, broad linewidths, and the unusual shape of the spectrum, the fitting of these two bands has not been completed.

We could, however, generate a simulated spectrum using our fitting program and compare it to the experimental spectrum. Rotational constants obtained from *ab initio* calculations for the perpendicular 1-methoxynaphthalene are A" = 1464.12, B" = 924.01, and C" = 590.42 MHz, respectively, in the ground state. These constants were then used to simulate the spectrum, varying only the rotational constants for the excited state during the simulation. A typical example is shown in Figure 11. The rotational constants for the excited state are A' = 1371.32, B' = 865.27, and C'= 555.52 MHz, respectively, and the rotational temperature is estimated to be 60
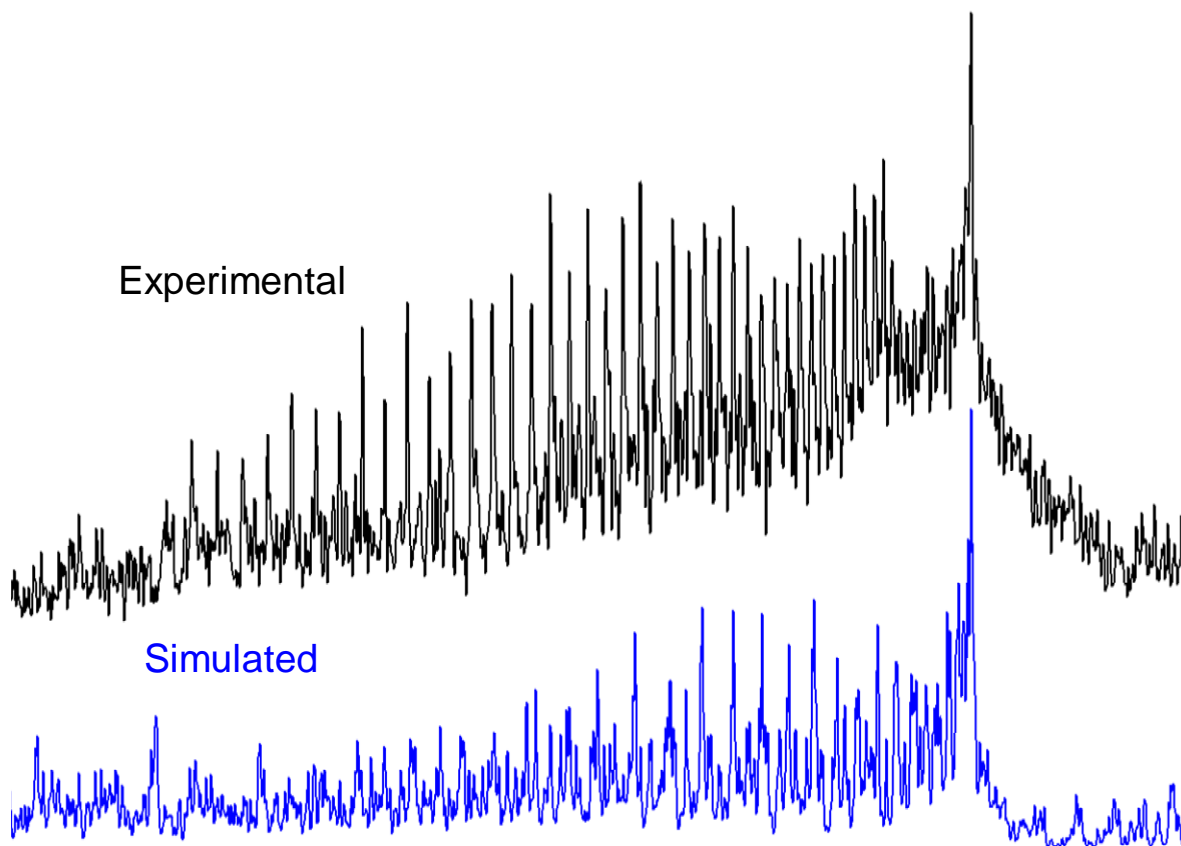
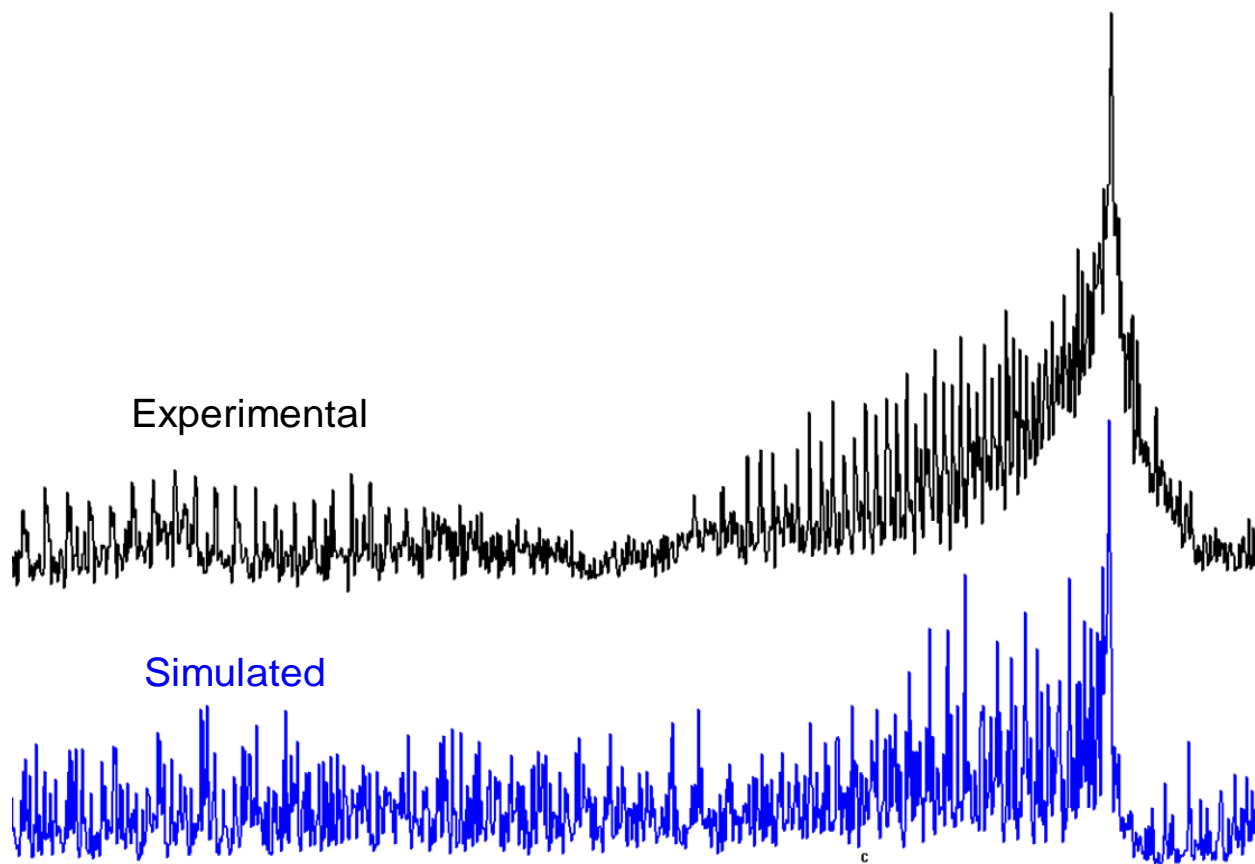**Figure 11. Comparision of observed and simulated spectra, –70 cm⁻¹ band.**

K. The simulated spectrum reproduces the sharp strong peak in the high wavenumber region and shows no significant peaks in the blue region. A significantly high rotational temperature was required to reproduce the peak intensity ratio between the strong sharp peak and the long series of peaks. But it fails to reproduce the pattern of the long series of peaks. Instead of having separations varying from 340 to 950 MHz, the simulated spectrum has separations varying from 660 to 2000 MHz with several small peaks between each relatively strong peak. The Gaussian linewidths are 26 MHz when He was used as a carrier gas; the Lorentzian linewidths were estimated to be 50 MHz to reproduce the approximate 80 MHz linewidths in the experimental spectrum.

Another simulation was performed with the same rotational constants used to simulate the -70 cm^{-1} band, varying only the rotational constant A' for the excited state during the simulation. A spectrum with A' = 1378.27 MHz at the rotational temperature at 60 K at different origin is compared to the $+16$ cm^{-1} band in Figure 12. This simulated spectrum reproduces the general shape of the experimental spectrum; a sharp strong peak at high wavenumbers, a long series of peaks in the R branch, and relatively small peaks in the P branch. But it also shows some peaks in the middle of the spectrum which are missing in the experimental spectrum. It also fails to reproduce the separation between peaks.

Although the fitting is incomplete yet, there are significant similarities between the experimental and simulated spectra. Also, the similarity between the -70 cm^{-1} band and the $+16$ cm^{-1} band indicates that they might come from same conformer.

Experimental

Simulated

Figure 12. Comparision of observed and simulated spectra, +16 cm^{-1} band.

2.4.   Discussion

For *trans*-1-methoxynaphthalene, the Lorentzian linewidth was determined to be 13 MHz. Since the Lorentzian component is related to the lifetime, τ, of the upper state by

$$\tau = \frac{1}{2\pi\Delta\nu}$$

which is derived from the uncertainty principle, the lifetime of the excited state of *trans*-1-methoxynaphthalene can be obtained from the relation, yielding a value of 12 nsec. This should be compared to the lifetimes of *trans*-2-methoxynaphthalene of 49 nsec and *cis*-2-methoxynaphthalene of 28.6 nsec [11].

The *a* axis of *trans*-1-methoxynaphthalene makes an angle of ~37° with respect to the molecular long axis due to the contribution from the heavy methoxy group, as shown in Fiure 13. Now, for a molecule to interact with an electromagnetic field and make a transition between two states, it must possess a dipole oscillating at the corresponding frequency for the transition. This transition moment (TM) between states with wavefunction ψ_i and ψ_f is defined as

$$\mu_{fi} = \int \psi_f^* \mu \psi_i d\tau$$

where μ is the electric dipole moment operator. The orientation of the TM gives information about the spatial properties of the wavefunctions of the two electronic states. In particular, the TM vector is oriented in the direction of electronic charge migration or displacement during
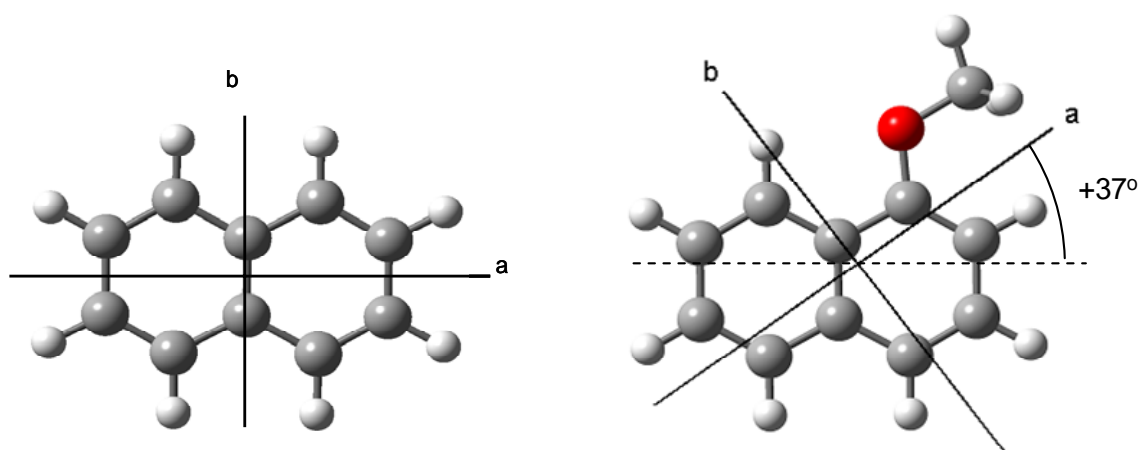
Figure 13 Inertial axes of naphthalene and *trans*-1-methoxynaphthalene.
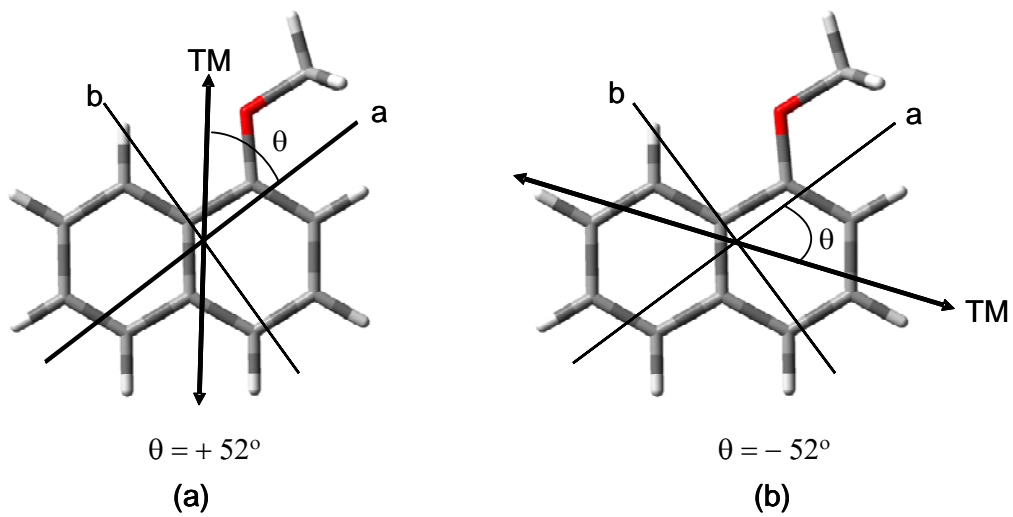
the transition.

The transition moment orientation can be determined from the intensities of the different subbands in the spectrum. The origin band of *trans*-1-methoxynaphthalene is an *ab* hybrid band; no *c*-type character was necessary to fit the spectrum. Thus, the orientation of the TM vector can be determined from the ratio of *a, b* type intensities using the following equation:

$$\tan^2 \theta = \frac{I_b}{I_a}$$

Here, θ is the angle between the transition moment vector and the *a* inertial axis of the molecule. The experimental result showed 38% *a*-type character and 62% *b*-type character from the intensity fit. This gives a transition moment angle $\theta = 52^o$, tilted from the *a* inertial axis as shown in Figure 14. There are two possible orientations of the transition moment vector depending on its sign; one is the TM vector lying almost parallel to the short axis of the molecule (Figure 14(a)), and the other is the TM vector lying almost parallel to the long axis of the molecule (Figure 14(b)).

Experimentally, the TM vector orientation could be determined from the spectrum of a van der Waals complex with Ar or He, or isotope exchange of the methoxy hydrogen with deuterium. But still we can speculate about the TM vector orientation using molecular orbital theory and other high resolution studies of naphthalene and its derivatives.

The $S_1 \leftarrow S_0$ transition of naphthalene is well known for its accidental near cancellation of transition moments. Majewski *et al.* [16] reported a weak parallel *a*-type transition for the $S_1 \leftarrow S_0$ transition of naphthalene in a high resolution LIF study. With substitutions on the naphthalene

Figure 14. Possible orientations of the experimental TM vector of *trans*-1-methoxynaphthalene.

ring, the transition moments no longer cancel, and the $S_1 \leftarrow S_0$ transition gains strength as observed from 1-fluoronaphthalene [17]. These authors reported that the spectrum of 1-fluoronaphthalene has 75% *a*-type character and 25% *b*-type character, indicating that the transition moment is rotated away from the *a* inertial axis by an angle of $\pm 30^o$. Johnson *et al.* [18] reported that the transition moment is tilted by $\pm 33^o$ from the *a* inertial axis for the $S_1 \leftarrow S_0$ transition of *trans*-1-hydroxynaphthalene, while the transition moment is tilted by $\pm 6^o$ from the *a* inertial axis for *cis*-1-hydroxynaphthalene. The difference in the two angles depends on the orientation of the lone pair orbital of oxygen relative to the naphthalene frame. Then, later, Humphrey, *et al.* [19] reported that the transition moment is tilted by -33° from the *a* inertial axis for the $S_1 \leftarrow S_0$ transition of the *trans*-1-hydroxynaphthalene, determined from $S_1 \leftarrow S_0$ fluorescence spectrum of *trans*-1-hydroxynaphthalene·NH_3 complex. This makes the transition moment tilted by -17° from the molecular long axis for *trans*-1-hydroxynaphthalene. For *trans*-1-methoxynaphthalene, one possible orientation of the transition moment, a -52° tilt from the *a* inertial axis (-15° tilted from molecular long axis), shows a similar transition moment orientation to *trans*-1-hydroxynaphthalene, with respect to the molecular long axis.

Figures 15 and 16 show the theoretical transition moments of *trans*-1-methoxynaphthalene for the $S_1 \leftarrow S_0$ transition and $S_2 \leftarrow S_0$ transition, respectively, calculated by the CIS/6-31G** method. According to the MO theory, the $S_1 \leftarrow S_0$ transition is due to the orbital mixing of the one-electron ϕ_5(HOMO) to ϕ_7(LUMO+1) and ϕ_4(HOMO-1) to ϕ_6(LUMO) transitions. The degree of orbital mixing for the $S_1 \leftarrow S_0$ transition is 62 % of HOMO to LUMO+1 transition, and a 38 % of HOMO-1 to LUMO transition. The calculated TM vector lies parallel to the long axis of the molecule. Comparing these predictions with experiment, we see that the orientation of the TM in *trans*-1-methoxynaphthalene is -52°.
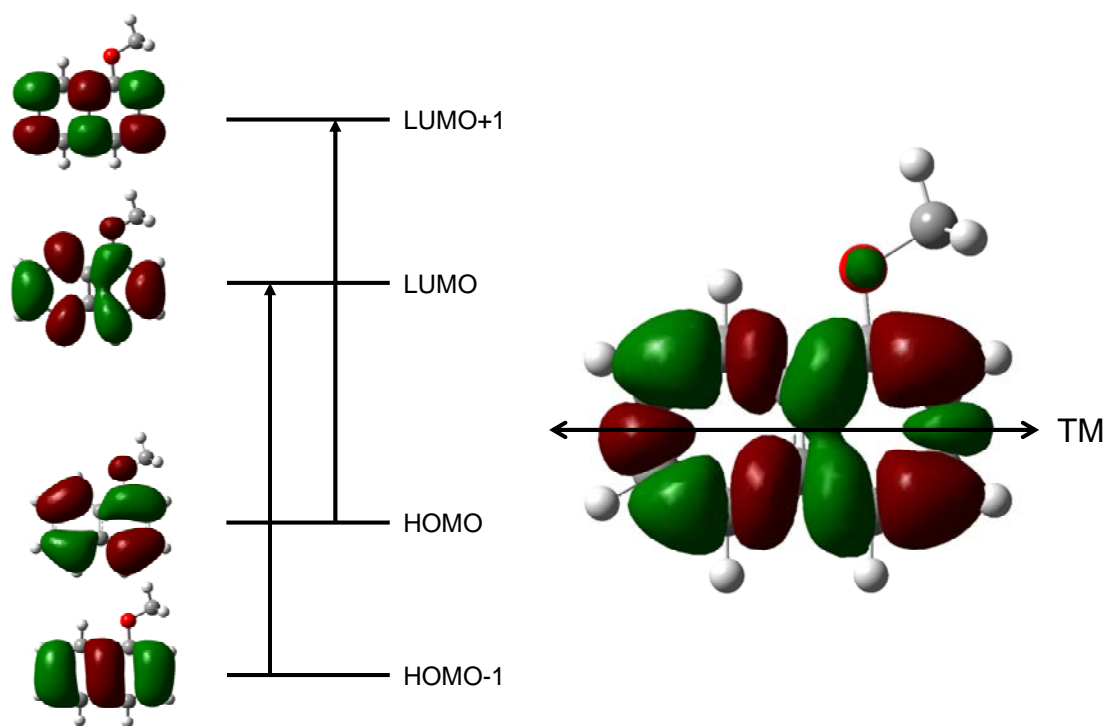
Figure 15. Theoretical transition moment of *trans*-1-methoxynaphthalene for the $S_1 \leftarrow S_0$ transition.
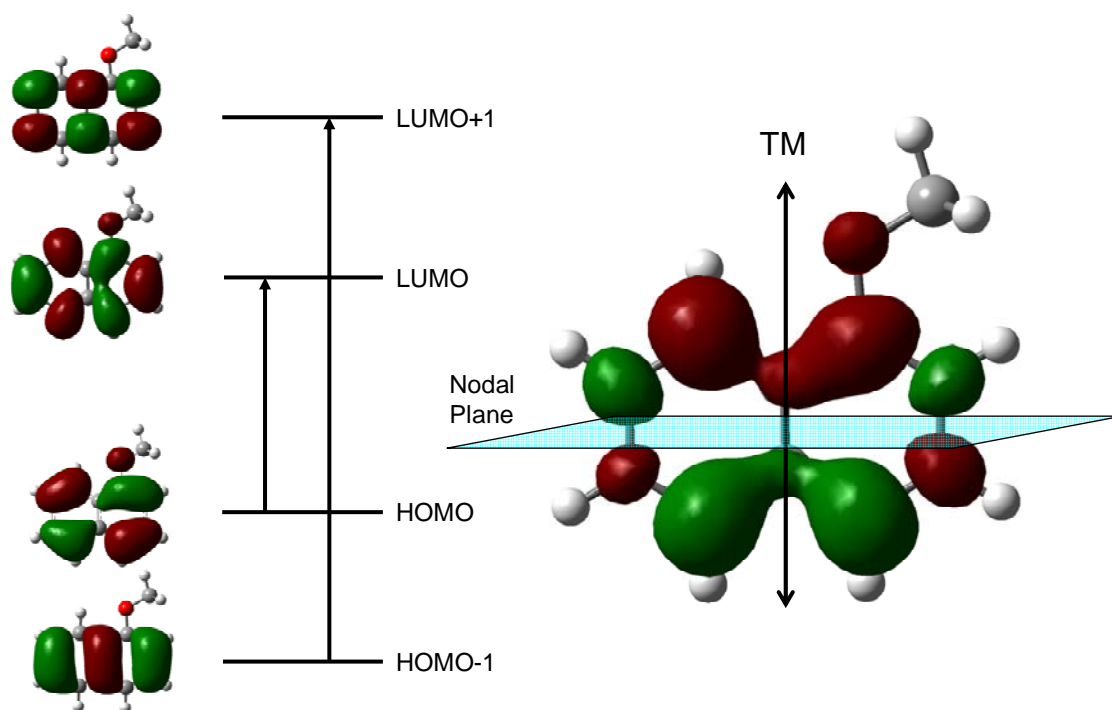
Figure 16. Theoretical transition moment of *trans*-1-methoxynaphthalene for the $S_2 \leftarrow S_0$ transition.

The tilting of the TM from the molecular long axis could be explained in two ways. One is a contribution from the other transitions whose transition moments are oriented along the molecular short axis. The HOMO to LUMO transition from $S_2 \leftarrow S_0$ transition can be a possibility for this contribution because the TM is parallel to the molecular short axis as shown in Figure 16. Another cause of the tilting could be a mixing with the lone pair electrons of the oxygen atom, as in the case of *trans*-1-hyroxynaphthalene [18, 19].

The unusual shapes of the spectra of the -70 cm^{-1} band and of the $+16$ cm^{-1} band can be ascribed to band head formation. When the rotational constants of the ground and excited states change upon excitation, the rotational levels in one state diverge with increasing J more slowly than in the other state. Then, the transition wavenumbers become closer as J increases and at a point, the transition wavenumber at $J+1$ is smaller than at J. The convergence of the transition wavenumber near this point forms a sharp, strong band head. For the case of a simple diatomic molecule, J_{rev}, the value of J at the reversal point, is given by $J_{rev} = (B''-3B')/2(B'- B'')$ for R branch transitions, and $J_{rev} = (B''+B')/2(B'- B'')$ for P branch transitions [20]. For a symmetric or near symmetric rotor, it is more complicated. Q branch heads occur when $\bar{B}' \approx \bar{B}''$, where $\bar{B} = (B+C)/2$. R branch heads form when $\bar{B}' < \bar{B}''$ and J_{rev} is given by $(\bar{B}''-3\bar{B}')/2(\bar{B}'-\bar{B}'')$. P branch heads form when $\bar{B}' > \bar{B}''$, and J_{rev} is given by $J_{rev} = (\bar{B}''+\bar{B}')/2(\bar{B}'-\bar{B}'')$ [20]. When one or more of the rotational constants between ground and excited state are significantly different, heads can form at low J. When the rotational constants are not very different, heads form at high J.

The populations of rotational energy levels are obtained from Boltzmann distribution as

$$N_J/N_0 = (2J + 1)exp(-E_r/kT)$$

where E_r is the rotational energy and *2J + 1* represents the degeneracy without electric or magnetic fields. Head formations are not often observed in jet beam studies because the rotational temperature is low, around 3 ~ 5 K using Ar as a carrier gas. When the temperature increases the population at high *J* increases and head formation may be observed. In case of the – 70 cm^{-1} band and the +16 cm^{-1} band in our experiments, He was used as a carrier gas at very low backing pressures implying that the temperature is high, which may allow us to observe the formation of the head. A rotational temperature of 60 K was used for the simulated spectrum in Figures 7 and 8. Different simulations also generated band heads at lower temperature, but the shape of the overall spectrum was different from the experimental spectrum. J_{rev} of the simulated spectrum is about $J = 15$, and the population at $J = 15$ is still large enough to form a band head. But after the reversal point, a long series of peaks was not observed. For this reason, higher rotational temperatures were used for the simulations shown in Figures 7 and 8.

From the discussion so far, we know that the theoretical rotational constants for the perpendicular conformer produce a simulated spectrum similar to the experimental spectrum. Therefore, we may say that –70 cm^{-1} band is the origin of perpendicular conformer.

Although there is no other direct evidence for the second conformer of 1-methoxynaphthalene, theoretical calculations give some insights into this possibility. Single point energy calculations done by Mahato, *et al*. [14] predict a perpendicular conformer as the second stable conformer. Our geometry optimization calculations agreed with this prediction. The possibility of *cis* conformer can be excluded due to the steric hindrance between the methyl group and the hydrogen atom at the C_8 position. Geometry optimizations for *cis*-1-

methoxynaphthalene was performed both in the ground state and excited state at the MP2 level with 6-31G** basis set, and the final structure returned to perpendicular conformer after the optimization, indicating that its *cis* conformer was too unstable to exist. Geometry optimizations for the perpendicular conformer did not return to the most stable *trans* conformer, unlike the case of the *cis* conformer, and this indicates that perpendicular conformer is also stable enough to exist at a local mimimum of the potential curve. The energy difference between the *trans* conformer and the perpendicular conformer was calculated to be 2.45 kcal/mol in our geometry optimization calculation, which is 0.35 kcal/mol larger than the previous single point energy calculation.

The possibility of the perpendicular conformer can be better understood by referring to the geometrical parameters provided by Mahato, *et al.* [14]. The labeling of the molecule is shown below:
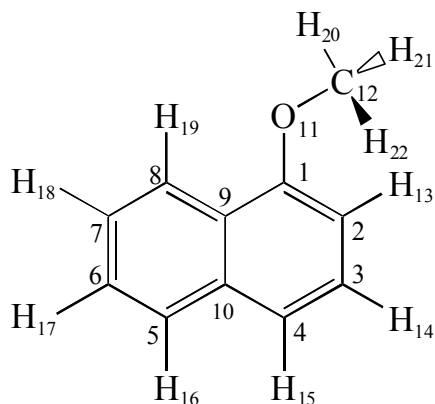
For the geometry optimized *trans* conformer in the ground state, the angle $\angle C_9$-C_1-O_{11} is 114.5^o, smaller than 120°, and the angle $\angle C_2$-C_1-O_{11} is 124.8^o, larger than 120°. This is due to the steric hindrance between methoxy group and hydrogen at C_2 which pushes the methoxy group away from the hydrogen. Also this opens up the angle $\angle C_1$-O_{11}-C_{12} to 116.5^o which is larger than 109°, the angle expected for sp^3 hybridization of the oxygen atom. This steric hindrance is relieved by

the rotation of the methoxy group. For the geometry optimized perpendicular conformer in the ground state, the angle $\angle C_9\text{-}C_1\text{-}O_{11}$ is 118.7^o, and the angle $\angle C_2\text{-}C_1\text{-}O_{11}$ is 120.0^o. Also the angle $\angle C_1\text{-}O_{11}\text{-}C_{12}$ is decreased to 111.7^o. The distance between the methoxy carbon and the C_2 hydrogen atom is now increased from 2.501 Å to 3.198 Å. Although there is less favorable bonding between C_1 and O (the bond length is increased from 1.371 Å (*trans*) to 1.387 Å (perpendicular)), and between C_{12} and O (the bond length is increased from 1.423 Å (*trans*) to 1.431 Å (perpendicular)), minimization of steric hindrance compensates for this energy increase enough for the perpendicular conformer to exist as a second stable conformer.

The *ab initio* calculation also provides more information about the nature of the blue shifted band at +16 cm^{-1} from the origin of the *trans* conformer. Since this band is blue shifted from the origin bands of both the *trans* conformer and the perpendicular conformer, the possibility of a hot band from these conformers can be excluded. Another possibility for this band is a high vibronic band of the *trans* conformer or the perpendicular conformer. *Ab initio* calculations of the vibronic frequencies of both conformers were performed at HF/6-31G** level. The result for the *trans* conformer shows that the first vibrational frequency appears at 139.6 cm^{-1} from the origin; there is no possible matching vibrational frequency for *trans* conformer around 16 cm^{-1}. But the result for the perpendicular conformer shows torsional vibration of methyl group at 61.5 cm^{-1} from the origin. It is possible that the +16 cm^{-1} band is torsional vibrational band of the perpendicular conformer. The similarity of the spectral shape between this band and the perpendicular conformer band also supports this possibility. Since they are populated from same ground state, their experimental rotational constants for ground state have to be the same, and this could be proved by fitting these two spectra later.

2.5.   Summary

We have observed and analyzed the rotationally resolved $S_1 \leftarrow S_0$ fluorescence excitation spectra of the origin of *trans*-1-methoxynaphthalene, using a high resolution laser spectrometer operating in the ultraviolet. The *trans*-1-methoxynaphthalene origin band is an *ab* hybrid band with 38% *a*-type character and 62% *b*-type character. The $S_1 \leftarrow S_0$ transition moment vector was determined to make an angle of $\pm 52^\circ$ with the *a* inertial axis. The rotational constants for *trans*-1-methoxynaphthalene are A" = 1643.98, B" = 832.62, C" = 554.83 MHz in the ground state, and A' = 1626.6, B' = 818.5, and C'= 546.6 MHz in the excited state. Rotationally resolved fluorescence excitation spectra of two weak bands at +16 cm^{-1} and –70 cm^{-1} from the origin band of *trans*-1-methoxynaphalene were also taken and analyzed. These bands exhibit unusual band head shapes. Even though the fits of these two bands are not complete yet, the possibility of perpendicular conformer was discussed both experimentally and theoretically.

2.6.   Acknowledgements

2.7.   References

[1] Majewski, W. A.; Pfanstiel, J. F.; Plusquellic, D. F.; Pratt, D. W. *Laser Techniques In Chemistry*, John Wiley & Sons, Inc. **1995**, 101

[2] Allen, G.; Fewster, S. In *International Rotations in Molecules*; Orville Thomas, W. J., Ed.; Wiley: New York, 1974; Chapter 8

[3] Friege, H.; Klessinger, M. *Chem. Ber.* **1979**, *112*, 1614

[4] Owen, N. L.; Hester, R. E.; *Spectrochim Acta, Part A* **1969**, *25*, 343

[5] Schaefer, T.; Penner, G. H. *J. Mol. Struct. (THEOCHEM)* **1987**, *157*, 179

[6] Onda, M.; Tonda, A.; Mori, S.; Yamaguchi, I. *J. Mol. Struct.* **1986**, *144*, 47

[7] Eisenhardt, C. G.; Pietraperzia, G.; Becucci, M. *Phys. Chem. Chem. Phys.* **2001**, *3*, 1407

[8] Konschin, H.; Thlli, H.; Grundfelt-Forsius, C. *J. Mol. Struct.* **1981**, *77*, 51

[9] Nagy, L. T.; Jancarova, M. Chem. Papers **1985**, *39*, 289

[10] Anderson, G. M. III.; Kollman, P. A.; Domelsmith, L. N.; Houk, K. N. *J. Am. Chem. Soc.* **1979**, *101*, 2344

[11] Troxler, T.; Pryor, B. A.; Topp, M. R. *Chem. Phys.Lett.* **1997**, *274*, 71

[12] Johnson, J. R.; Jordan, K. D.; Plusquellic, D. F.; Pratt, D. W. *J. Chem. Phys.* **1990**, *93*, 2258

[13] Lakshminarayan, C.; Knee, J. L. *J. Phys. Chem.* **1990**, *94*, 2637

[14] Mahato, K. K.; Das, A.; Panda, A. N.; Chakraborty T.; Sathyamurthy, N. *J. Phys. Chem.* **2002**, *106*, 12058

[15] Das, A.; Mahato, K. K.; Chakraborty T. *J. Chem. Phys.* **2001**, *114*, 8310

[16] Majewski, W. A.; Meerts, W. L. *J. Mol. Spec.* **1984**, *104*, 271

[17] Majewski, W. A.; Plusquellic, D. F. ; Pratt, D. W. *J. Chem. Phys.* **1989**, *90*, 1362

[18] Johnson, J. R.; Jordan, K. D. ; Plusquellic, D. F.; Pratt, D. W. *J. Chem. Phys.* **1990**, *93*, 2258

[19] Humphrey, S.; Pratt, D. W. *J. Chem. Phys.* **1996**, *104*, 8332

[20] Hollas, J. M. *High Resolution Spectroscopy*, Wiley **1998**

BIBLIOGRAPHY

Chapter 1

[1] Majewski, W. A.; Pfanstiel, J. F.; Plusquellic, D. F.; Pratt, D. W. *Laser Techniques In Chemistry*, John Wiley & Sons, Inc. **1995**, 101

[2] Majewski, W. A.; Plusquellic, D. F.; Pratt, D. W. *J. Chem. Phys.* **1989**, *90*, 1362

[3] Gerstenkorn, S. ; Luc, P. *Atlas du spectroscopie d'absorption de la molecule d'iode*, CNRS, Paris, **1978** and **1982**

[4] Demtroder, W. *Laser Spectroscopy*, Springer-Verlag, Berlin Heidelberg, **1982**

Chapter 2

[1] Majewski, W. A.; Pfanstiel, J. F.; Plusquellic, D. F.; Pratt, D. W. *Laser Techniques In Chemistry*, John Wiley & Sons, Inc. **1995**, 101

[2] Allen, G.; Fewster, S. In *International Rotations in Molecules*; Orville Thomas, W. J., Ed.; Wiley: New York, 1974; Chapter 8

[3] Friege, H.; Klessinger, M. *Chem. Ber.* **1979**, *112*, 1614

[4] Owen, N. L.; Hester, R. E.; *Spectrochim Acta, Part A* **1969**, *25*, 343

[5] Schaefer, T.; Penner, G. H. *J. Mol. Struct. (THEOCHEM)* **1987**, *157*, 179

[6] Onda, M.; Tonda, A.; Mori, S.; Yamaguchi, I. *J. Mol. Struct.* **1986**, *144*, 47

[7] Eisenhardt, C. G.; Pietraperzia, G.; Becucci, M. *Phys. Chem. Chem. Phys.* **2001**, *3*, 1407

[8] Konschin, H.; Thlli, H.; Grundfelt-Forsius, C. *J. Mol. Struct.* **1981**, *77*, 51

[9] Nagy, L. T.; Jancarova, M. Chem. Papers **1985**, *39*, 289

[10] Anderson, G. M. III.; Kollman, P. A.; Domelsmith, L. N.; Houk, K. N. *J. Am. Chem. Soc.* **1979**, *101*, 2344

[11] Troxler, T.; Pryor, B. A.; Topp, M. R. *Chem. Phys.Lett.* **1997**, *274*, 71

[12] Johnson, J. R.; Jordan, K. D.; Plusquellic, D. F.; Pratt, D. W. *J. Chem. Phys.* **1990**, *93*, 2258

[13] Lakshminarayan, C.; Knee, J. L. *J. Phys. Chem.* **1990**, *94*, 2637

[14] Mahato, K. K.; Das, A.; Panda, A. N.; Chakraborty T.; Sathyamurthy, N. *J. Phys. Chem.* **2002**, *106*, 12058

[15] Das, A.; Mahato, K. K.; Chakraborty T. *J. Chem. Phys.* **2001**, *114*, 8310

[16] Majewski, W. A.; Meerts, W. L. *J. Mol. Spec.* **1984**, *104*, 271

[17] Majewski, W. A.; Plusquellic, D. F. ; Pratt, D. W. *J. Chem. Phys.* **1989**, *90*, 1362

[18] Johnson, J. R.; Jordan, K. D. ; Plusquellic, D. F.; Pratt, D. W. *J. Chem. Phys.* **1990**, *93*, 2258

[19] Humphrey, S.; Pratt, D. W. *J. Chem. Phys.* **1996**, *104*, 8332

[20] Hollas, J. M. *High Resolution Spectroscopy*, Wiley **1998**